Article

Application of Bio-Inspired Gold Nanoparticles as Advanced Nanomaterial in Halt Nociceptive Pathway and Hepatotoxicity via Triggering Antioxidation System

Rehman Ullah [1,*], Sakina Bibi [1], Muhammad Nauman Khan [2,3], Amal M. Al Mohaimeed [4], Qirat Naz [5] and Asif Kamal [6,*]

[1] Department of Botany, Faculty of Life and Environmental Sciences, University of Peshawar, Peshawar 25120, Pakistan; sakinabibi06@gmail.com
[2] Department of Botany, Islamia College Peshawar, Peshawar 25120, Pakistan; nomiflora@uop.edu.pk
[3] University Public School (UPS), University of Peshawar, Peshawar 25120, Pakistan
[4] Department of Chemistry, College of Science, King Saud University, P.O. Box 22452, Riyadh 11495, Saudi Arabia; muhemeed@ksu.edu.sa
[5] Department of Business and Creative Industries, University of South Wales, Newport NP18 3QT, UK
[6] Department of Plant Sciences, Faculty of Biological Sciences, Quaid-i-Azam University, Islamabad 45320, Pakistan
[*] Correspondence: rehmanbotany@uop.edu.pk (R.U.); kamal@bs.qau.pk (A.K.)

Abstract: This study aimed to investigate the pharmacological efficacy of gold nanoparticles (GNs) synthesized using a green route, employing the rhizome extract of *Euphorbia wallichii* (REEW) as a bioreductant and surface stabilizing agent. The GNs were characterized by a series of complementary analytical techniques including SEM-EDX, XRD, DLS, and IR spectroscopy. The reducing ability of REEW and synthesis of GNs were confirmed using UV–visible absorption spectroscopy, and the presence of spherical GNs with an fcc geometry was further confirmed through SEM and XRD analyses. The role of REEW's extract as a stabilizing agent towards GNs was verified through FTIR and electronic absorption spectral measurement. The GC-MS analysis showed the presence of 41 different phytochemicals in REEW (chloromethyl 2-chloroundecanoate; cortisone; benzo[h]quinolone; piperidine, 2,4-dimethyl- 3,6,7-trimethoxyphenanthroindolizidine; 4-methyl-; 2-[2-quinolylmethyleneamino]ethanol, etc.), with RT values ranging from 3.10 to 27.22 min. The REEW-functionalized GNs exhibited promising antioxidant efficacy against H_2O_2 and $^*OH$ used as probe molecules. DPPH scavenging test showed significant EC_{50} values of 19.47 µg/mL, 13.53 µg/mL, and 10.57 µg/mL at 30, 60, and 90 min of incubation, respectively. Thermal nociceptive mice significantly acquired analgesia in a dose-dependent manner. Moreover, pre-treatment with REEW-GNs significantly restored serum ALT, AST, ALT, T.P, and Bilirubin levels in PCM-intoxicated mice. The antidiabetic activity in alloxan-induced diabetic rabbits fell in orders of metformin > GNs 300 mg/kg b.w > GNs 200 mg/kg b.w > GNs 100 mg/kg b.w > saline at 0.1 h of drug administration. To sum up, REEW functionalized GNs have tremendous potential for curing degenerative/metabolic diseases caused as a result of oxidative stresses.

Keywords: gold nanoparticles; hepato-protective; anti-diabetic; analgesic; antioxidant; spasmolytic

1. Introduction

Nano-biotechnology is an emerging frontier in the medical field that exploits the application of nano-sized material for targeted cell or tissue-specific clinical interventions. Nanotechnology seeks to design and employ techniques for the synthesis of nano-systems that can interact at the molecular (sub-cellular) level with great specificity to achieve maximum therapeutic potency with minimal side effects [1]. Owing to their small sizes and controllable morphologies, unique size, and shape-dependent novel properties, the applications of nanomaterials, particularly metallic NPs, are continuously and rapidly

growing in various technological sectors and scientific fields [2,3]. Metallic nanoparticles (NPs) are especially of great interest because of their improved size/shape-dependent catalytic, electronic, and optical properties [4]. From an application and biocompatibility point of view, the synthesis of nanomaterial through greener and biologically friendly routes using safe and low-cost reactants is of great interest. For instance, the synthesis of metallic NPs using microbes and/or plant extracts can potentially eliminate the problems of biocompatibility caused by synthetic reducing agents, which are often toxic, such as sodium borohydride and hydrazine. The green synthetic route provides progression over the chemical route as the former is eco-friendly and cost-effective. Many plants and microbes have been found to be excellent sources of natural reducing agents [5]. Biomimetic synthesis of metallic NPs using phyto-extracts as reducing and stabilizing agents is not only cost-effective but also minimizes the threats of environmental hazards. The use of plant extract for nanoparticle synthesis is advantageous over other biological processes because it eliminates the elaborated process of maintaining cell cultures and can be adapted for large-scale preparations [6]. Phytochemicals such as phenolic compounds, terpenoids, and alkaloids have been found to be suitable reducing agents with high efficiency [7]. Among the metal NPs, the synthesis and applications of gold nanostructures in various fields of science and technology have attracted special attention during the last several years [8]. In recent years, gold nanoparticles (GNs) have attracted much attention due to their unique properties such as high surface area, high biocompatibility, and stability, which make them suitable for various applications including catalysis, drug delivery, and biomedical imaging [8,9]. Important application areas of GNs include drug delivery systems, biosensing, bio-diagnostics, cancer photo-thermal therapy, and catalysis [10–16]. Such diverse applications of GNs stem from their unique physicochemical characteristics, such as intense SPR bands, thermal conductance, catalytic potential, biochemical stability, anti-angiogenic anti-arthritic, antimicrobial, and anti-malarial activity [17,18]. Although AuNPs display exquisite potential in diagnosing and treating cancerous tumors, their biosafety is still a challenging issue that needs to be addressed. While many research studies have suggested that AuNPs have appropriate biocompatibility and in vivo protection, a few studies have suggested that they have toxic in vivo effects. These contradictory results may be due to the distinctive synthesis methods or the unique morphology, size, and structure of AuNPs. Therefore, the biosafety issues caused by the diverse properties of AuNPs need to be addressed prior to medical trials [19].

Euphorbia wallichii belongs to the family Euphorbiaceae, which includes herbs, shrubs, trees, and succulent plants, both wild and cultivated species, and are mainly distributed in tropical and temperate zones [19]. *Euphorbia wallichii*, commonly known as Wallich or Himalayan Spurge, is native to the Himalayas region of Pakistan in the north and extends eastward to the Chinese province Yunnan, between altitudes of 2200–4000 m. It is a perennial herb with a woody rootstock that can reach a height of up to 100 cm. The cyathium inflorescence is subtended by yellowish ovate bracts with a tricarpellary ovary. *Euphorbia wallichii* contains essential secondary metabolites, including flavonoids, alkaloids, diterpenoids, and triterpenoids [20]. Therefore, it has been extensively used as folk medicine by various ethnicities all over the globe [21,22]. The methanolic extract of *E. wallichii* has been previously used for the preparation of silver nanoparticles, which has shown significant inhibition of the selected bacterial and fungal pathogens [23]. Similarly, the ethanolic extract of *E. wallichii* rhizome was utilized as a bio-reductant for the synthesis of silver nanoparticles. The application of synthesized nanoparticles has shown potent biological activities and was found to be effective against pathogenic infectious and oxidative stress ailments [24].

2. Results and Discussion

2.1. Synthesis and Characterization of REEW-GNs

Biomimetic GNs were synthesized using the reducing method, where Au^{3+} was reduced by REEW's extract in a reaction medium containing an aqueous solution of 0.1 mM

HAuCl$_4$ and an aqueous solution (200 μg/mL) of REEW's extract in different ratios (1:1 to 1:4). The reaction medium turned from an initial light pale to the characteristic dark pinkish-purple color of GNs due to the collective oscillation of surface electrons (plasmons) of GNs in resonance with the light wave, a phenomenon called surface plasmon resonance. The electronic absorption spectroscopic measurement showed two important observations [7]. The electronic absorption spectroscopic measurement (Figure 1) showed two important observations. Firstly, the SPR band at around 535 nm confirmed the formation of GNs and the concentration of GNs was higher for a 1:1 mixture of HuCl$_4$ and REEW extract, as indicated by higher optical density for this sample in the characteristic range. Secondly, the absorption of the sample above 600 nm was reasonably lower, indicating the particles in the solution did not undergo intense agglomeration. However, some degree of aggregation was expected as absorption above 600 nm was not completely absent. The agglomerates shift λ1 up to 680 nm due to plasmonic coupling. Previous study has reported that gold nano-agglomerates exhibited a broad peak with a wavelength range of 650–700 nm, which is characteristic of such agglomerates [25].
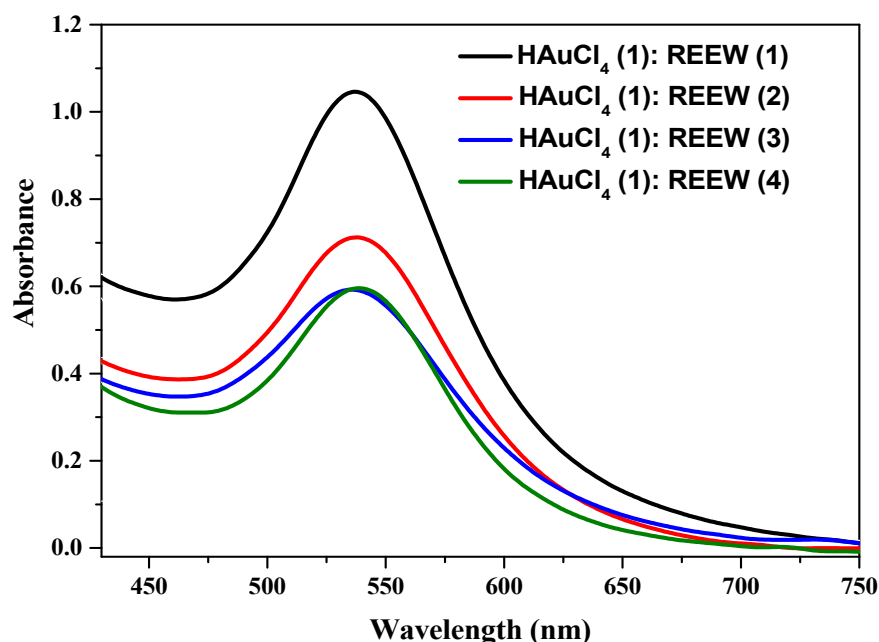
Figure 1. UV–visible absorption spectra of REEW-stabilized GNs suspension.

The SEM image confirmed the formation of spherical and spheroidal GNs with a variable size, ranging from 20–130 nm with a mean of 115 ± 12 nm (Figure 2a). Owing to the high surface-to-volume ratio of GNs, some aggregation was observed, but the use of REEW's extract seemed to stabilize the particles as individual spherical GNs were also observed in the SEM image. The presence of metallic gold in synthesized nanoparticles was confirmed by elemental analysis using energy-dispersive X-ray spectroscopy (EDS), which showed the characteristic X-ray emission peaks of Au (2.1 keV) in the EDS spectrum of the spherical particles observed in the SEM image (Figure 2b). The C and O signals were likely due to X-ray emission from carbohydrates/proteins present in plant extract [26]. The hydrodynamic size and surface charge of the colloidal REEW-GNs were analyzed using dynamic light scattering (DLS) and zeta potential measurements. The result of the zeta potential shown and DLS in Figure 2c,d, respectively, revealed a moderate to high polydispersity in size distribution with an average hydrodynamic size of 78 nm with a zeta potential of −18.1 mV.
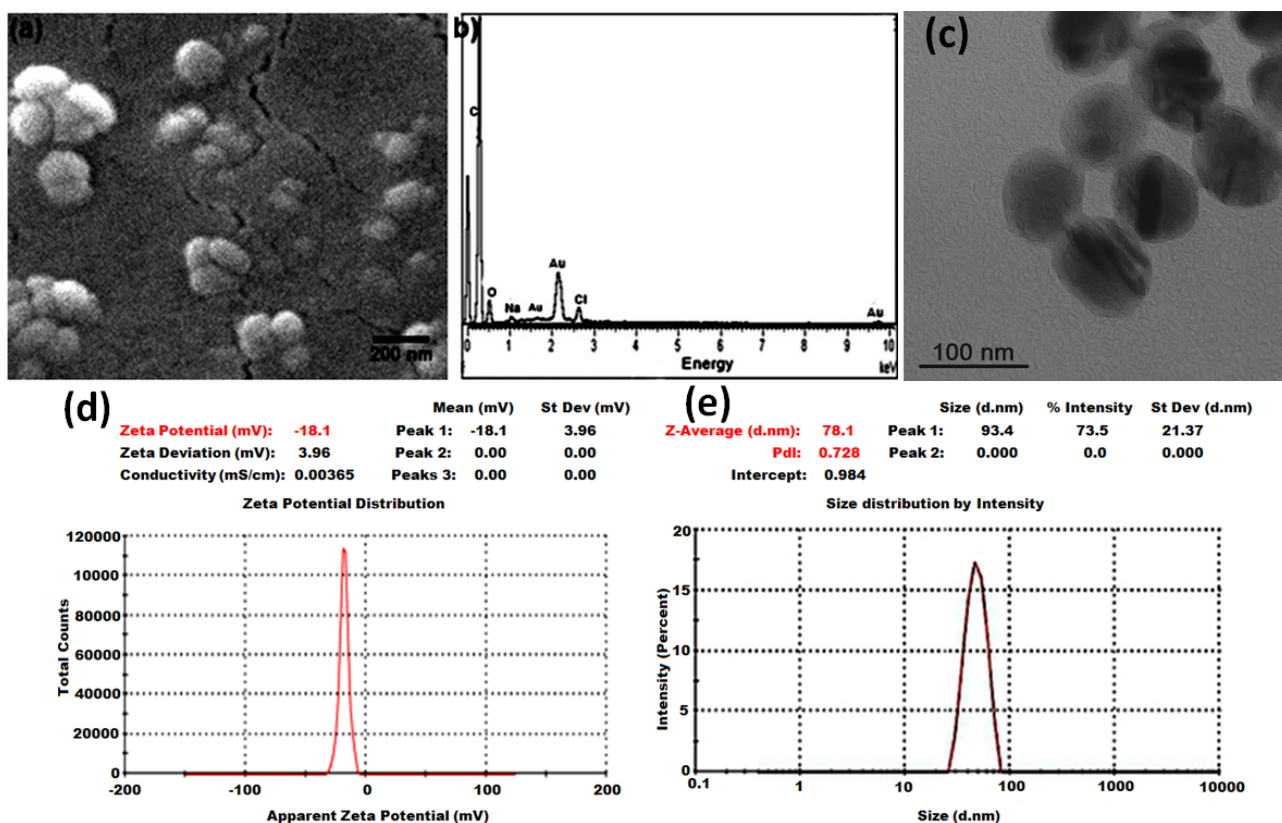
Figure 2. SEM and TEM of REEW-GNs showing spherical morphology (**a**,**c**) and EDX spectrum of REEW-GNs illustrating the elemental composition of the sample (**b**). Zeta potential of −18.1 mV (**d**) and average hydrodynamic diameter of 78.1 nm (**e**) of colloidal REEW-GNs are shown.

The X-ray diffraction (XRD) analysis of REEW-GNs exhibited distinct peaks at 2θ values 38.24°, 44.50°, 64.7°, 77.80°, and 77.92°, which corresponded to Bragg's planes (1 1 1), (2 0 0), (2 2 0), and (3 1 1) of gold, respectively. The diffraction pattern of GNs was in agreement with the standard diffraction pattern of the face-centered cubic (fcc) structure of crystalline Au (ICSD PFD no. 4-784) (Figure 3). The average crystallite size of GNs was determined by applying Scherrer's equation, which is based on the broadening of the (111) reflection and was found to be 19 nm.
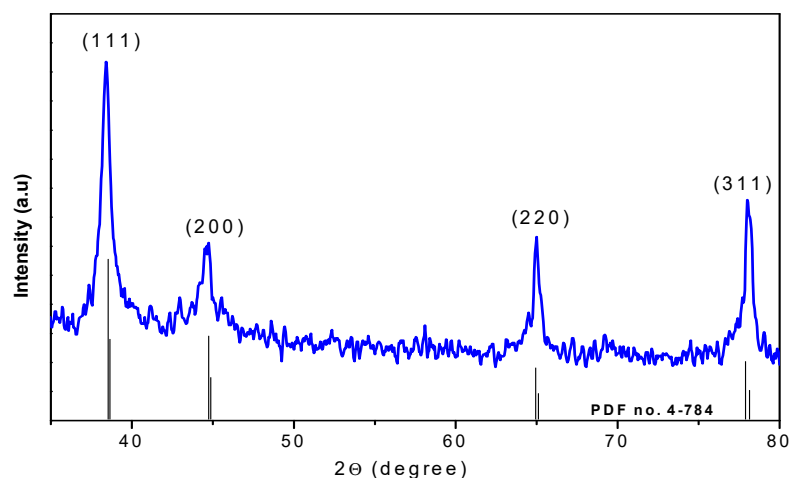
Figure 3. X-ray diffractogram of REEW-GNs: the standard diffraction pattern of Au (JCPDS PDF no 4-784) is also shown at the bottom.

FT-IR spectroscopy of REEW showed vibration stretch at 3277 and 3254 cm^{-1} representing O-H bond of polyphenols and/or alcohol, 2923 cm^{-1} representing C-H stretching of alkanes and/or fatty acyl, 2336 and 2323 cm^{-1} representing C≡N stretching may be attributed to cyanogenic glycosides (Figure 4). The vibrational stretching at 1754 cm^{-1} represents the C=O bond, 1531 cm^{-1} vibration is from N-H bending of 1° amines, 1186 cm^{-1}, and 1010 wave numbers cm^{-1} representing C-N and C-O stretches, respectively. The dislocation of O-H, C≡N, and C=O stretches in IR spectra of REEW-GNs was due to the reduction of gold ions by phytochemicals possessing these functional groups and/or stabilization of the reaction medium.
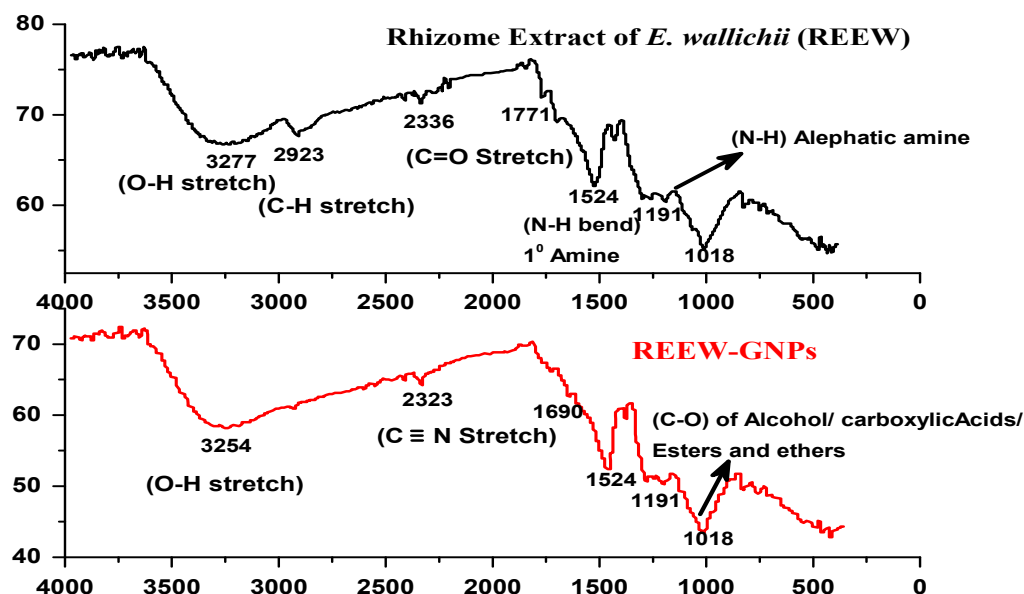
Figure 4. FTIR spectra of REEW and REEW-GNs showing various functional groups correspond to different vibration stretches.

2.2. GC-MS Analysis of REEW

The ethanol extract of rhizome of *Euphorbia wallichii* was screened for its phytochemical profiling using gas chromatography and mass spectrometry analysis. The GC-MS chromatogram (Figure 5) revealed the presence of 41 different peaks attributed to various phytochemicals at different retention times (min). GC-MS results were summarized in Table 1, which showed a total of 41 different compounds identified based on their retention times (RT), peak area, and molecular mass. The first peak with least RT vale of 3.10 min was for chloromethyl 2-chloroundecanoate with a molecular mass of 268 g/mol, followed by RT 3.84 min attributed to 1-formyl-2,2-dimethyl-3-cis-(2-methyl-but-2-enyl)-6-methylidene-cyclohexane. The maximum RT value of 27.22 min was recorded for benzo[h]quinoline, 2,4-dimethyl- followed by 2,4,6-Cycloheptatrien-1-one, 3,5-bis-trimethylsilyl with RT value of 26.79 min. The GC-MS analysis of REEW confirmed the presence of 3,6,7-trimethoxyphenanthroindolizidine; piperidine, 4-methyl-; 2-[2-quinolyl-methyleneamino]ethanol; cortisone and 3-(dimethylamino)-7-(methylamino)phenothiazin-5-ium, etc.

Table 1. GC-MS of ethanol extract of rhizome of *Euphorbia wallichii* (REEW) showing various phytochemicals.

| P.N	RT	Peak Area	Peak Height	Name of Compound	Structure	Mass Spectrogram	Chemical Formula (M.WT)
1.	3.1	1786.93	217.94	Chloromethyl 2-chloroundecanoate			$C_{12}H_{22}Cl_2O_2$ (268)
2.	3.84	15,548.58	491.52	1-Formyl-2,2-dimethyl-3-cis-(2-methyl-but-2-enyl)-6-methylidene-cyclohexane			$C_{15}H_{24}O$ (220)
3.	4.92	4067.5	212.68	3,6,7-Trimethoxyphenanthroindolizidine			$C_{23}H_{25}NO_3$ (363)
4.	5.26	1610.1	176.27	Proadifen			$C_{23}H_{31}NO_2$ (353)
5.	5.53	473.92	72.76	-(2-Acetoxyphenyl)-1-ethyl-3-methyl-5-(4-nitrophenyl)pyrazole			$C_{20}H_{19}N_3O_4$ (365)
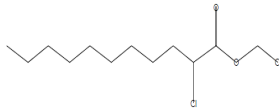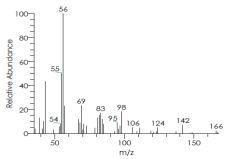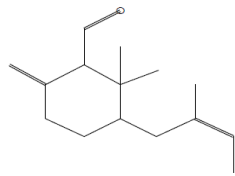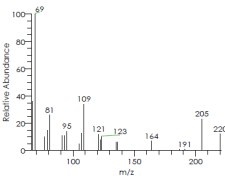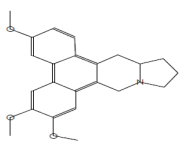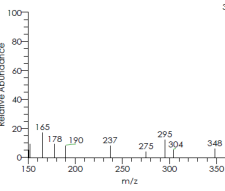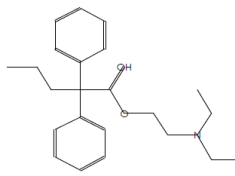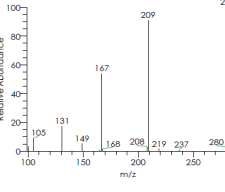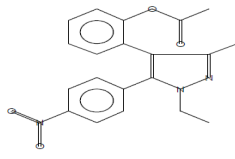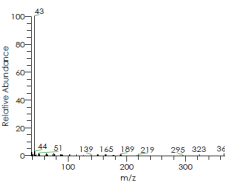
Table 1. *Cont.*

P.N	RT	Peak Area	Peak Height	Name of Compound	Structure	Mass Spectrogram	Chemical Formula (M.WT)
6.	5.79	1664.36	151.29	Piperidine, 4-methyl-			$C_6H_{13}N$ (99)
7.	6.08	736.93	84.66	Dihexyl phthalate			$C_{20}H_{30}O_4$ (334)
8.	6.69	6814.49	254.4	2-[2-Quinolylmethyleneamino]ethanol			$C_{12}H_{12}N_2O$ (200)
9.	7.42	2406.57	138.73	Ethyl 3-[1-(2,6-dichlorobenzoyl)-5-formylpyrrol-2-yl]prop-2-enoate			$C_{17}H_{13}Cl_2NO_4$ (365)
10.	7.75	1185.45	145.04	(2S,4S)-2,4-Dimethylundecanedioic acid dimethyl ester			$C_{15}H_{28}O_4$ (272)
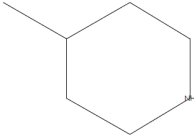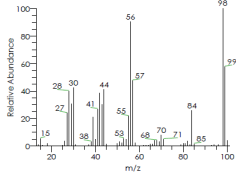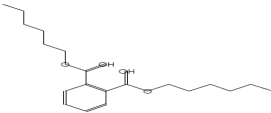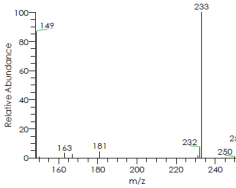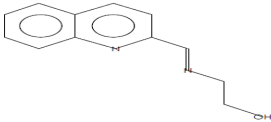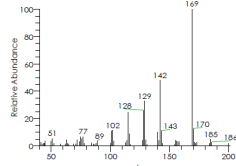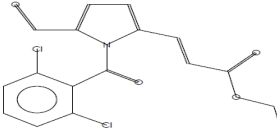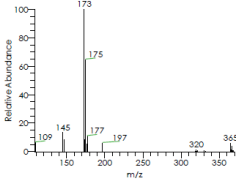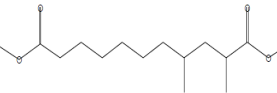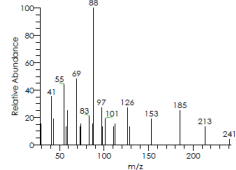
Table 1. *Cont.*

P.N	RT	Peak Area	Peak Height	Name of Compound	Structure	Mass Spectrogram	Chemical Formula (M.WT)
11.	8.4	5948.04	249.16	Dichlorofluorescein			$C_{20}H_{10}Cl_2O_5$ (400)
12.	9.13	6484.75	357.23	Cortisone			$C_{21}H_{28}O_5$ (360)
13.	9.85	4942.7	293.1	Curan-17-ol, 19,20-didehydro-, (19E)-			$C_{19}H_{24}N_2O$ (296)
14.	10.15	3154.45	237.43	Difenoconazol			$C_{19}H_{17}Cl_2N_3O_3$ (405)
15.	10.66	2591.58	159.94	cyanazine [M+H]+15			$C_9H_{13}ClN_6$ (240)
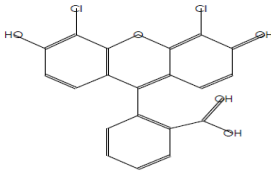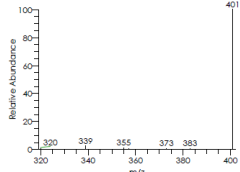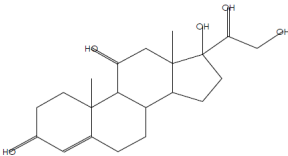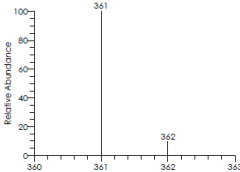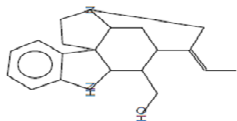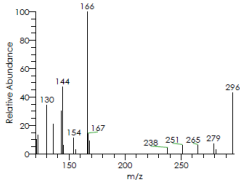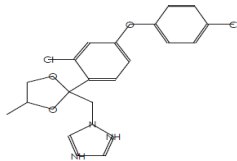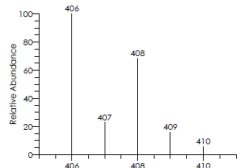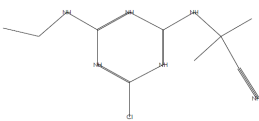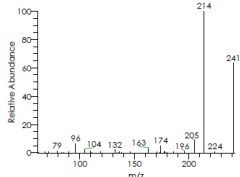
Table 1. *Cont.*

| P.N	RT	Peak Area	Peak Height	Name of Compound	Structure	Mass Spectrogram	Chemical Formula (M.WT)
16.	11.17	6316.54	471.62	Chlorbromuron			$C_9H_{10}BrClN_2O_2$ (292)
17.	11.8	8776.81	293.21	3-(Dimethylamino)-7-(methylamino)phenothiazin-5-ium			$C_{15}H_{16}N_3S$ (270)
18.	12.62	6330.37	241.84	2-Methyl-9-nitro-7-oxo-4,5,6,7-tetrahydroimidazo(4,5,1-jk)benzodiazepine-1,4			$C_{11}H_{10}N_4O_3$ (246)
19.	13.51	2165.13	108.41	Acetic acid, trifluoro-, (9,10-dihydro-1,8-dimethoxy-9,10-dioxo-2-anthracenyl)methyl ester			$C_{19}H_{13}F_3O_6$ (394)
20.	14.1	6260.98	202.11	Methyl 4-hydroxybutyl phthalate			$C_{13}H_{16}O_5$ (252)
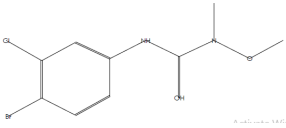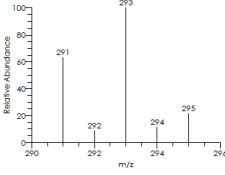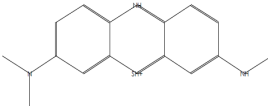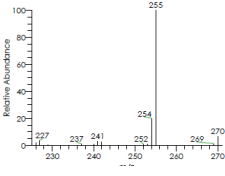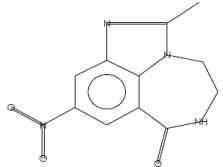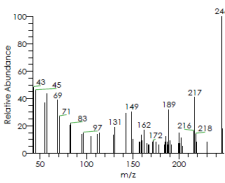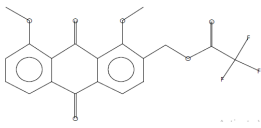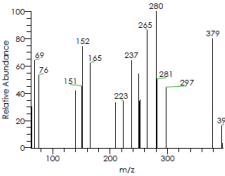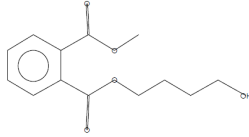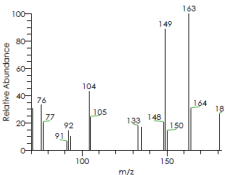
Table 1. *Cont.*

P.N	RT	Peak Area	Peak Height	Name of Compound	Structure	Mass Spectrogram	Chemical Formula (M.WT)
21.	15.04	2948.07	163.44	3-Bromo-thiophene-2-carboxamide			C_5H_4BrNOS (205)
22.	15.65	3239.99	224.82	Difenoxin			$C_{28}H_{28}N_2O_2$ (424)
23.	16.42	2058.57	147.06	[1,1′-Biphenyl]-4-carbonitrile, 4′-ethyl-			$C_{15}H_{13}N$ (207)
24.	16.97	3934.14	267.28	2-(4-Bromobutyl)-furan			$C_8H_{11}BrO$ (202)
25.	18.14	8657.45	261.62	2,5-Dimethyl-1-pyrroline			$C_6H_{11}N$ (97)
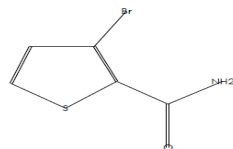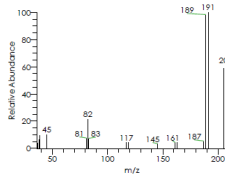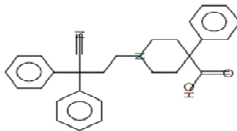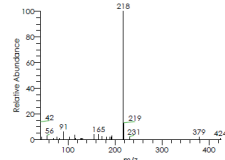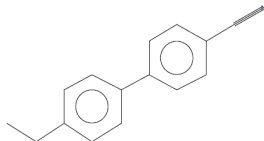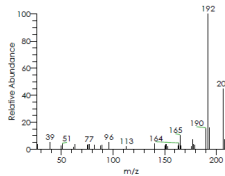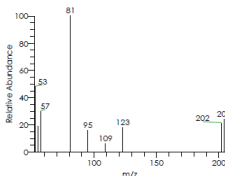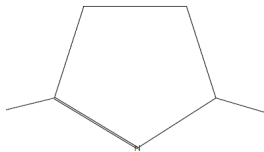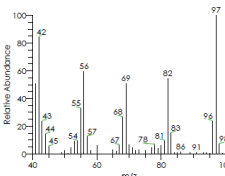
Table 1. *Cont.*

| P.N	RT	Peak Area	Peak Height	Name of Compound	Structure	Mass Spectrogram	Chemical Formula (M.WT)
26.	18.89	2297.94	178.23	7,12a-Dimethyl-1,2,3,4,4a,11,12,12a-octahydrochrysene			$C_{20}H_{24}$ (264)
27.	19.24	3725.55	262.34	Lupan-3-one, cyclic 1,2-ethanediyl acetal			$C_{32}H_{54}O_2$ (470)
28.	19.68	6469.64	311.58	Pyrrolidine, 3,3-dimethyl-1,2,2-triphenyl-			$C_{24}H_{25}N$ (327)
29.	20.21	2098.38	214.64	Androstane-3,7,12,17-tetrol, 7,12-diacetate, (3à,5á,7à,12à,17á)-			$C_{23}H_{36}O_6$ (408)
30.	20.89	9622.97	622.2	2,5-Methanofuro[3,2-b]pyridine-4(2H)-carboxylic acid, hexahydro-8-[[(4-methylphenyl)sulfonyl]oxy]-, ethyl ester, (2à,3aá,5à,7aá,8R*)-			$C_{18}H_{23}NO_6S$ (381)
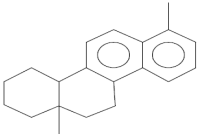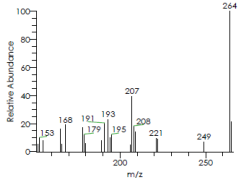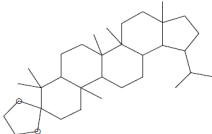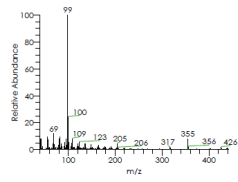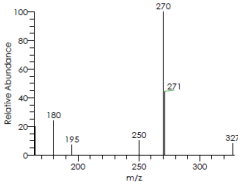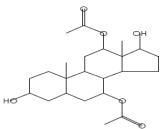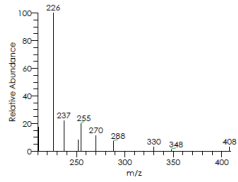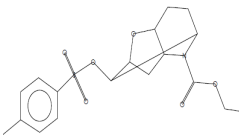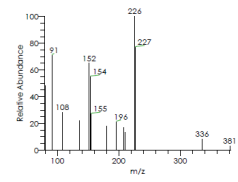
Table 1. *Cont.*

P.N	RT	Peak Area	Peak Height	Name of Compound	Structure	Mass Spectrogram	Chemical Formula (M.WT)
31.	21.29	15,590.39	673.31	4H-Pyran-3-carboxylic acid, 6-amino-5-cyano-4-(2-fluorophenyl)-2-methyl-, ethyl ester			$C_{16}H_{15}FN_2O_3$ (302)
32.	22.62	7233.17	565.72	2,4(1H,3H)-Pyrimidinedione, 5-bromo-6-methyl-3-(1-methylpropyl)-			$C_9H_{13}BrN_2O_2$ (260)
33.	23.25	20,022.39	607.85	Trimethyl [4-(1,1,3,3,-tetramethylbutyl)phenoxy]silane			$C_{17}H_{30}OSi$ (278)
34.	23.72	2039.02	259.57	2-Propen-1-one, 1,3-diphenyl-			$C_{15}H_{12}O$ (208)
35.	24.06	7347.26	616.22	Quinomethionate			$C_{10}H_6N_2OS_2$ (234)
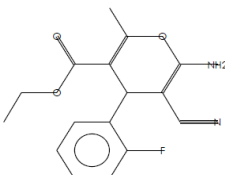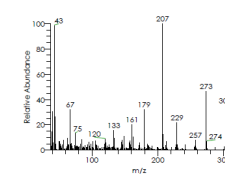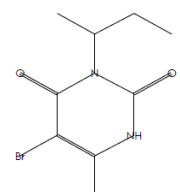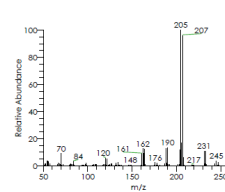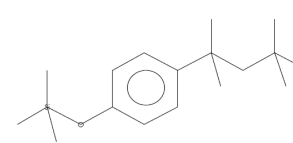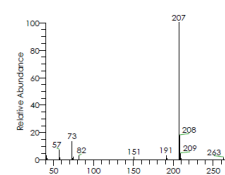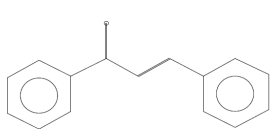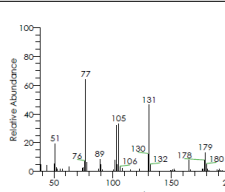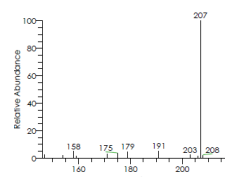
Table 1. *Cont.*

P.N	RT	Peak Area	Peak Height	Name of Compound	Structure	Mass Spectrogram	Chemical Formula (M.WT)
36.	24.45	4952.8	376.19	2-[3-(4-tert-Butyl-phenoxy)-2-hydroxy-propylsulfanyl]-4,6-dimethyl-nicotinonitrile			$C_{21}H_{26}N_2O_2S$ (370)
37.	24.82	8712.46	691.84	Cyclotetrasiloxane, octamethyl-			$C_8H_{24}O_4Si_4$ (296)
38.	25.71	40,412.02	1326	-Hydroxy-7,8,9,10-tetramethyl-7,8-dihydrocyclohepta[d,e]naphthalene			$C_{18}H_{20}O$ (252)
39.	26.2	41,587.04	1445.5	Silicic acid, diethyl bis(trimethylsilyl) ester			$C_{10}H_{28}O_4Si_3$ (296)
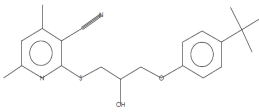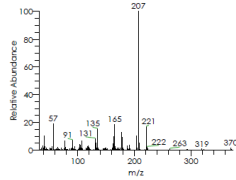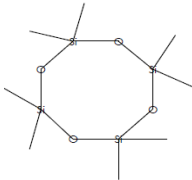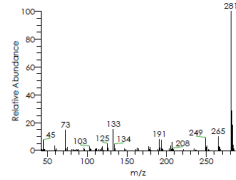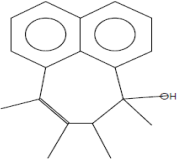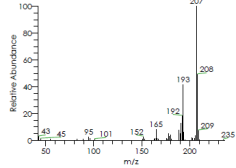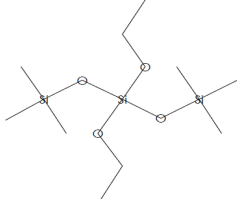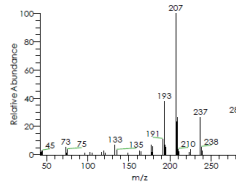
Table 1. *Cont.*

| P.N	RT	Peak Area	Peak Height	Name of Compound	Structure	Mass Spectrogram	Chemical Formula (M.WT)
40.	26.79	9879.32	832.02	2,4,6- Cycloheptatrien-1-one, 3,5-bis-trimethylsilyl-			$C_{13}H_{22}OSi_2$ (250)
41.	27.22	16,576.25	923.56	Benzo[h]quinoline, 2,4-dimethyl-			$C_{15}H_{13}N$ (207)
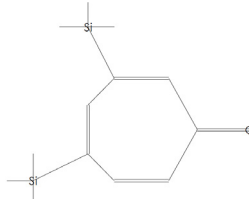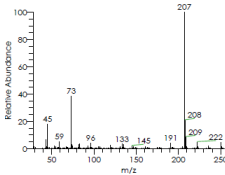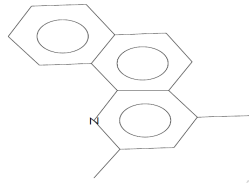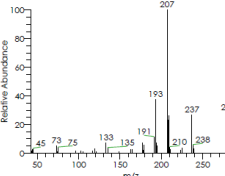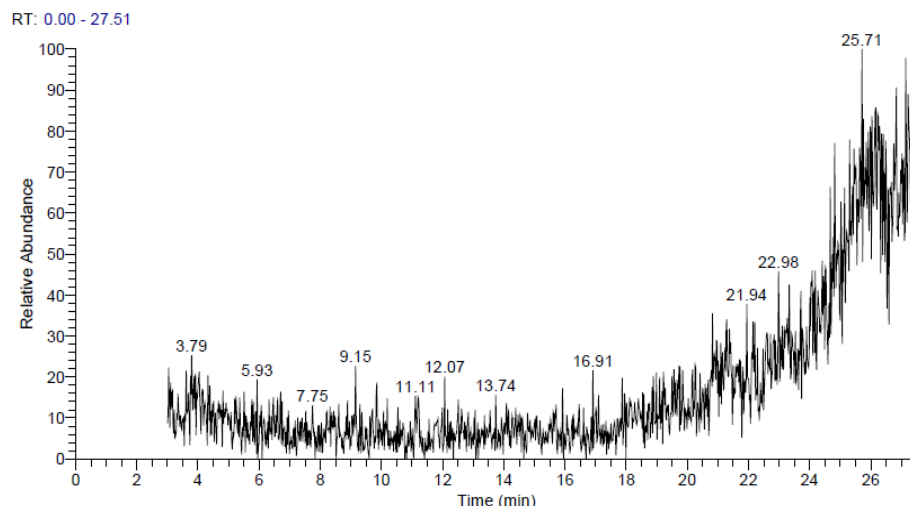
Figure 5. GC-MS chromatogram of alcoholic extract of Rhizome of *Euphorbia wallichii*.

2.3. Biological Efficacy of REEW-GNs

2.3.1. OH Scavenging Assay (Fenton Assay)

Phenol red oxidation assay was employed to characterize the potential of REEW-GNs to scavenge $^\bullet$OH radicals generated by the Fenton process, $Fe^{2+} + H_2O_2 \rightarrow Fe^{3+} + {}^\bullet OH + OH^-$, where $^\bullet$OH is a highly reactive oxidant, involved in a broad range biochemical oxidation reactions and other low-temperature oxidation processes. Figure 6 showed the potential of REEW-GNs to protect phenol red in solution from $^\bullet$OH oxidation. The dye treated with REEW-GNs showed a higher absorbance compared to the dye without REEW-GNs, confirming the antioxidant potential of REEW-GNs. The antioxidant activity of GNs is attributed to secondary metabolites such as polyphenols and glycosides present in REEW as evidenced by FTIR spectroscopy. These natural products act as metal chelates and/or reducing agents towards $^\bullet$OH and thus exhibit antioxidant activity. $^\bullet$OH radical is one of the major reactive oxygen species (ROSs) causing lipid peroxidation, which is formed in the biosystem via Fenton's reaction, causes molecular damage, and leads to degenerative diseases such as carcinogenesis, Parkinson's disease, brain ischemia, and hepatitis, etc. [27]. Thus, our current findings suggest that REEW-GNs have a protective potential for biosystems from oxidative stresses by scavenging ROSs.
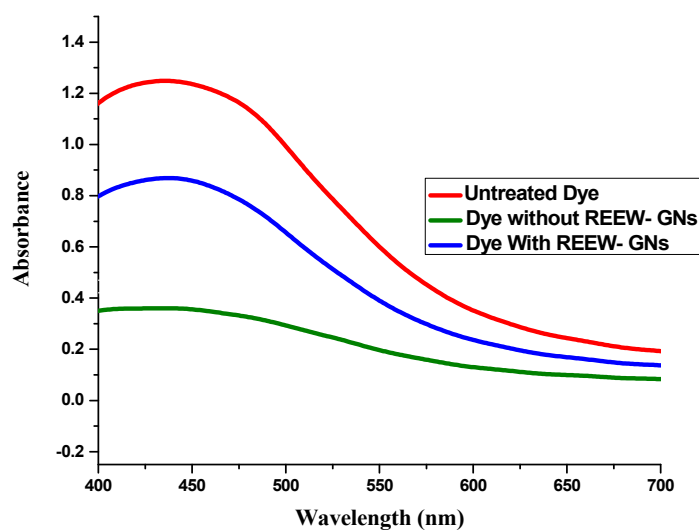
Figure 6. Absorption spectra of phenol red as target/probe molecule to study the $^\bullet$OH scavenging activity of REEW-GNs: the spectra of phenol red dye with and without REEW-GNs are shown for comparison.

2.3.2. H_2O_2 Scavenging Assay

Hydrogen peroxide (H_2O_2) is not highly reactive towards biomolecules but can be a strong ROS when converted to $^{\bullet}OH$ by interaction with a transition metal or UV light [28]. Adding H_2O_2 to cells leads to transition metal ion-dependent $OH^{\bullet}$–mediated oxidative DNA damage as well as the liberation of iron from hemoglobin [29]. Natural products such as flavonoids, polyphenols, and alkaloids have scavenging potentials for these ROSs. In the current study, the H_2O_2 scavenging efficacy of REEW-GNs was evaluated in comparison with ascorbate, a standard antioxidant drug. Figure 7 revealed a dose-dependent inhibition of H_2O_2 by REEW-GNs and ascorbate. All experimental doses of ascorbate showed better antioxidant effects against H_2O_2 than its counterpart REEW-GNs. This might be due to the capping of some phytochemicals not exhibiting significant scavenging of H_2O_2 but adding bulk to the GNs surface. The antioxidant natural products in REEW absorb onto the surface of GNs, which have a high surface-to-volume ratio, and thus effectively interact and scavenged H_2O_2 molecules. In tissues, electron reduction of O_2 primarily forms superoxide anion, which is then enzymatically or spontaneously converted to H_2O_2. It is widely considered that H_2O_2 is toxic in vivo and must be rapidly eliminated, employing enzymes such as catalases, peroxidases, and thioredoxin-linked systems [30].
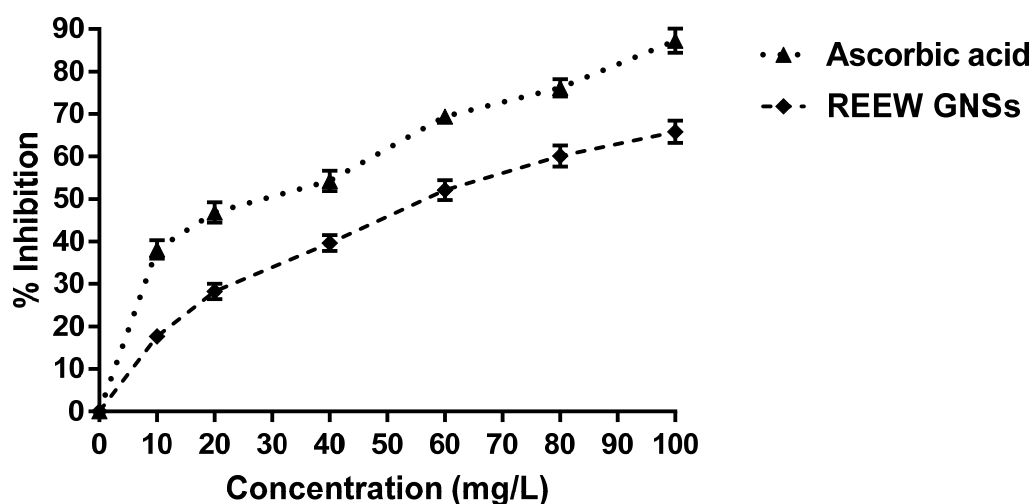
Figure 7. H_2O_2 scavenging assay of REEW-GNs and ascorbic acid (standard), showing percent H_2O_2 inhibition at various experimental doses.

2.3.3. DPPH Scavenging Assay

DPPH is a free radical with central nitrogen, and upon reduction, its color changes from violet to yellow. DPPH is thought to be a lipophilic radical where a chain reaction is initiated by lipid auto-oxidation [31,32]. The reducing potential of REEW-GNs was quantified spectroscopically by determining the change in color of DPPH. Figure 8 shows that ascorbate evidently bleached DPPH, hence showing minimum absorption in the 500–600 nm region. Likewise, REEW-GNs scavenged DPPH by bleaching its purple color in a dose-dependent manner (Figure 7). The effective concentrations ($EC_{50s,\ 70s,\ and\ 90s}$) of DPPH scavenging by GNs and ascorbate at different reaction times are summarized in Table 2. For 30, 60, and 90 min of reaction times, the effective concentrations of GNs and ascorbate for 50% of DPPH scavenging were 19.47, 13.53, 10.57 µg/mL and 3.46, 2.86, and 1.64 µg/mL, respectively. During the synthesis process, GNs were capped by various functional groups present in REEW, which have the capacity to donate hydrogens or electrons and scavenge DPPH. Being natural electron donors, these phytochemicals do not lead to the formation of free radicals upon oxidation as: $AH + R^{\bullet} \rightarrow RH + A$ where A do not propagate the free radical chain reaction and stabilize the structures by resonance.
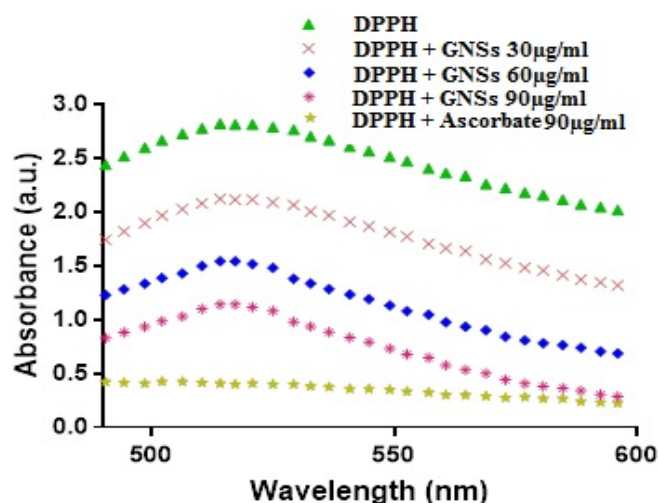
Figure 8. DPPH scavenging assay at various experimental doses of REEW-GNs and ascorbic acid (standard) as measured by acquiring absorption spectra in the 500–600 nm range.

Table 2. DPPH radical scavenging potential of REEW-GNs in comparison with ascorbic acid at different reaction times.

Treatments	Reaction Time (Min)	EC_{50} (µG/mL)	(EC_{50}) 95% CL	EC_{70} (µG/mL)	EC_{90} (µG/mL)	Probit
	30	19.47	9.63–28.36	118.21	1607.24	Y = 4.14 + 0.68X
REEW-GNS	60	13.53	4.96–21/35	88.69	1343.91	Y = 4.27 + 0.64X
	90	10.57	2.73–18.14	79.37	1464.05	Y = 4.39 + 0.60X
	30	3.46	1.03–6.43	11.399	63.861	Y = 4.45 + 1.01X
ASCORBATE	60	2.86	0.75–5.60	9.32	51.36	Y = 4.53 + 1.02X
	90	1.64	0.20–4.03	6.07	40.49	Y = 4.80 + 0.92X

Note: "EC" represent effective concentration for scavenging a defined mole (in percent) of DPPH. "CL" shows confidant limit of EC at $p = 0.05$.

2.3.4. Evaluation of Antidiabetic Activity

As mentioned earlier, the antidiabetic activity of REEW-GNs was evaluated in alloxan-induced diabetic rabbits. The antidiabetic activity in alloxan-induced diabetic rabbits falls in orders of; metformin > GNs 300 mg/kg b.w > GNs 200 mg/kg b.w > GNs 100 mg/kg b.w > saline after 0.1 h of drugs administration, metformin > GNs 300 mg/kg b.w > GNs 100 mg/kg b.w > GNs 200 mg/kg b.w > saline after 2 h, metformin > GNs 300 mg/kg b.w > GNs 200 mg/kg b.w > GNs 100 mg/kg b.w > saline after 4 h of administration and GNs 300 mg/kg b.w > metformin > GNs 200 mg/kg b.w > GNs 100 mg/kg b.w > saline after 8th and subsequent hours of drugs administrations. One-way ANOVA revealed significant hypoglycemia in alloxan diabetic rabbits at all experimental doses of GNs compared to the saline (control) condition. The pattern of antidiabetic potential was inclined till 2 h of drug administration followed by a decline in subsequent hours except for GNs at 200 mg/kg b.w, which showed inclined antidiabetic potential till the 8th hour of administration (Figure 9). Alloxan tends to inhibit the synthesis of proinsulin thus causing IDDM or NIDDM by damaging nucleic acid and reducing the NAD content of pancreatic beta cells. The pronounced antidiabetic activity of GNs may be associated with an insulin-stimulating effect by restoration of pancreatic beta-cells [33]. Sulfur-containing phytochemicals (alkaloids, flavonoids, etc.), of REEW capping GNs show a tendency for the inhibition of chemical species competing with insulin for their SH group. Phytochemicals, such as alkaloids and polyphenols, which stabilize gold nanoparticles (GNs), can significantly help in restoring normal conditions by combating the oxidative stress caused by alloxan treatment [34].
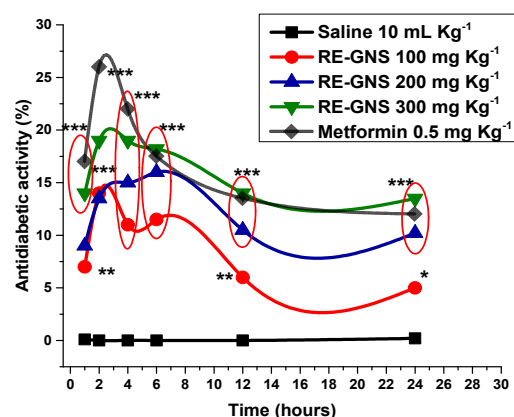
Figure 9. Antidiabetic effect of various doses of REEW-GNs at different time intervals: percent reduction in blood glucose level (BGL) is represented as mean ± SEM of $n = 6$ at $p < 0.05$. OWANOVA revealed significant to highly significant BGL reduction compared to saline. ** and *** represent highly significant effect compared to saline ($p < 0.01$), * represents significant effect ($p < 0.05$) where NS represents statistically non-significant differences among the treatments.

2.3.5. Antinociceptive Efficacy

The antinociceptive efficacy of REEW-GNs was determined using Eddy′s hot plate method in Swiss albino mice. Figure 10 shows a highly significant ($p < 0.01$) attenuation of nociception in experimental animals by GNs compared to saline (control) conditions. In the paw flick modal, REEW-GNs significantly elevated latency time (seconds) at all the experimental doses (100, 200, and 300 mg/kg b.w) after 30, 60, and 90 min of drug administration. At 30 min of oral administration of GNs at a dose of 100, 200, and 300 mg/kg b.w caused evident analgesia (percent of diclo. Na) by 63.87%, 67.71%, and 74.33% of diclo. Na, at 60 min 64.66%, 84.13%, and 65.84% and at 90 min 63.13%, 61.88%, and 64.82%, respectively.
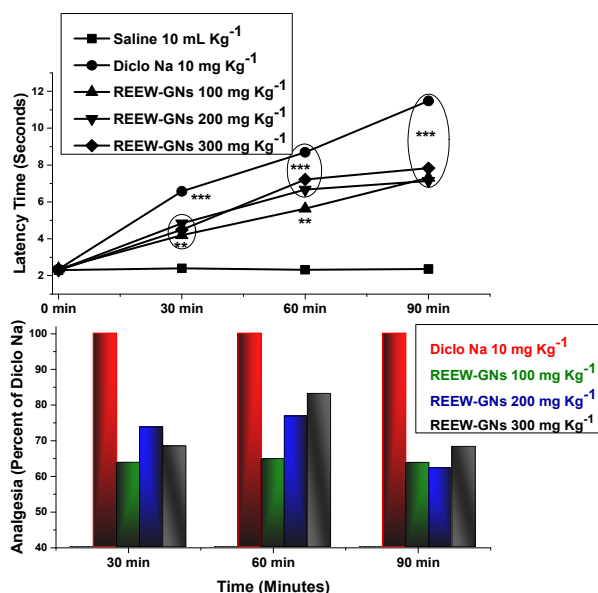
Figure 10. Analgesic effect of various doses of REEW-GNs at different time intervals: latency time (seconds) is represented as mean ± SEM of $n = 6$ at $p < 0.05$. OWANOVA revealed significant to highly significant elevation in latency time compared to saline. ** and *** represent highly significant effect compared to saline ($p < 0.01$).

Tissue damage causes pain either by stimulating nociceptive receptors or due to damage in neural structures without nociception (neuralgia). The former responds easily to analgesics, while neuralgia is very difficult to treat as it persists long after the initial injury

has healed [35,36]. Prostaglandins, serotonin, bradykinin, histamine, and leukotrienes are important mediators of nociception via a peripheral mechanism, tending to reduce the activation threshold for TTX-R Na channels via a protein kinase A pathway. Opiate, serotonergic, and dopaminergic descending noradrenergics are central systems, modulating pain through complex processes [37]. In the thermal nociception test, pre-oral administration of REEW-mediated GNs caused evident dose-related analgesia, although less effective than Diclo Na. Thermal nociceptive tests are more sensitive to opioid μ-agonists. Thus, our study suggests the involvement of μ-opioid receptors mediated by GNs results in an analgesic response through the central mechanism [38]. The analgesic effect of some herbal remedies has been attributed to their active secondary metabolites (alkaloids, flavonoids, saponins, tannins, etc.), for stalling prostaglandins and histamine biosynthesis [39,40]. It should be noted that IR spectroscopy of REEW suggested the functional groups associated with these secondary metabolites, capping GNs, involved in hindering nociception mediators.

2.3.6. Hepato-Protective Assay

The administration of acetaminophen (PCM) at a dose of 1 g/kg b.w, causes a significant increase in serum levels of ALP, AST, ALT, and bilirubin, which serve as biochemical markers for liver function. This increase is attributed to hepatonecrosis, induced by PCM, which results in the release of these enzymes into the bloodstream as reported earlier [41,42]. Both silymarin and REEW-GNs exhibited hepatoprotection by significantly ($p < 0.05$) reducing serum ALT, AST, ALP, and bilirubin levels in experimental mice compared to the acetaminophen (PCM) treated group. Animals treated with 100, 250, and 500 mg/kg b.w of GNs showed mean serum ALP levels of 185.69 IU/L, 171.61 IU/L, and 160.19 IU/L compared to an elevated serum ALP level of 246.33 IU/L in the PCM treated group. Similar trends were observed for AST, ALT, and bilirubin as well. PMC intoxication induced a significant ($p < 0.05$) reduction in serum total protein (T.P) content in experimental animals. Silymarin and REEW-GNs at 100, 250, and 500 mg/kg b.w, significantly restored serum T.P content by 2.93 g/dL and 2.27 g/dL, 2.51 g/dL, and 2.57 g/dL, respectively, in PCM intoxicated mice with mean T.P of 1.83 g/dL (Figure 11).

(**A**)   (**B**)
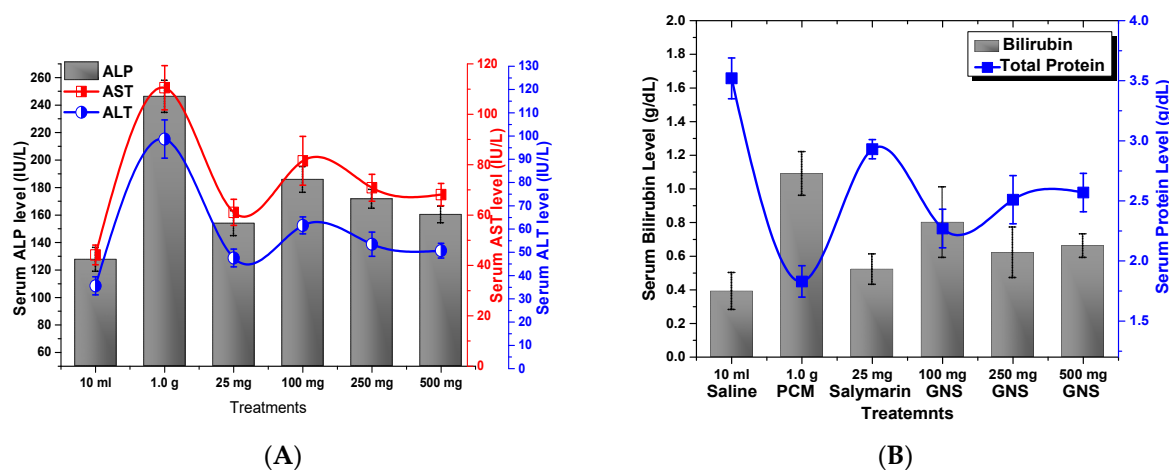
Figure 11. Hepato-protective effect of various doses of REEW-GNs and silymarin in acetaminophen (paracetamol) intoxicated mice. Values represent mean effect ± SEM of *n* = 6, serum ALP, AST, and ALT level (IU/L) (**A**), bilirubin and total protein level (g/dL) (**B**), statistically significant differences at *p* < 0.05.

Acetaminophen is itemized to induce acute hepatotoxicity at higher doses due to its bioactivation to a toxic electrophile, *N*-acetyl *p*-benzoquinone imine (NAPQI) by cytochrome P450 system, binds to cellular macromolecules, likely leading to lipoxidation or oxidize SH groups of amino acids residues of the protein, thus, altering the homeostasis of Ca^+ [43]. This results in oxidative stress and leads to the depletion of α-tocopherol

and glutathione, etc., resulting in peroxidation and alkylation of hepatic macromolecules. Depletion of α-tocopherol and glutathione and induction of cytochrome are the leading prompt factors to liver injury [44]. PCM altered hepatic activity, since ALT, AST, ALP, and bilirubin levels are elevated (Figure 11). Similarly, hypoalbuminemia depicts chronic liver dysfunction and a useful index of the severity of hepatocyte malfunction. Pretreated mice with REEW-GNs significantly declined serum ALT, AST, ALP, and bilirubin levels, thus restoring the liver physiology of PCM-intoxicated liver. The strong antioxidant potential of natural products capping GNs counteract the oxidative stress acquired due to PCM-induced injury and hence ensured hepatoprotection [45].

3. Materials and Methods

3.1. Synthesis of GNs

GNs were synthesized by reducing Au^{+3} to Au^0 using 70% ethanolic extract (*v/v*) of rhizome of *E. wallichii* (REEW) as reducing and stabilizing agent. A 0.1 mM aqueous solution of $HAuCl_4$ (Aldrich) was stirred with 200 μg/mL aqueous solution of REEW in different ratios (1:1 to 1:4) at 35 ± 3 °C until a change in color of reaction mixture from light pale to pinkish purple was observed.

3.2. Antioxidant Potential of REEW-Stabilized GNs

Antioxidant potential of REEW-GNs was evaluated using three different protocols.

3.2.1. DPPH Scavenging Assay

In the DPPH scavenging activity, 0.1 mM DPPH in 80% methanol was added to PBS (pH 7.4) followed by addition of different doses (10, 20, 40, 60, 80, and 100 μg/mL) of REEW-GNs, and the mixture was incubated for 90 min in dark. The optical density of each mixture was measured at 517 nm after different time intervals (30, 60, and 90 min of incubation) using a UV–Vis spectrophotometer. Untreated (pure) DPPH was used as a control while ascorbic acid was employed as a standard antioxidant drug. Antioxidant potential of REEW-GNs and ascorbate was measured as;

$$Antioxidant\ potential\ (\%) = \frac{Ac - At}{Ac} \times 100 \tag{1}$$

where A_c is absorbance shown by control and A_t is absorbance in test.

3.2.2. H_2O_2 Scavenging Assay

The ability of REEW-GNs to scavenge H_2O_2 was also evaluated. For this purpose, 1 mL of REEW-GNs or ascorbate (100 μg/mL) was added to a 50 mL solution of H_2O_2 (40 mM) in PBS (pH 7.4) and incubated for 20 min at room temperature. The absorbance of all test samples was measured at 230 nm using a UV–Vis spectrophotometer. Pure H_2O_2 in BPS was used as a control. The percent H_2O_2 scavenging activity was determined using Equation (1).

3.2.3. •OH Scavenging Assay (Fenton Assay)

The hydroxyl (•OH) free radical scavenging assay was performed using phenol red as a target molecule.

The effect of REEW-GNs on the discoloration rate of phenol red in the presence of •OH was measured as antioxidant potency. A reaction medium (10 mL, pH 6.2) containing REEW-GNs (100 μg/mL) in PBS (50 mM), Iron (II) chloride (0.5 μM), phenol red (0.1 mM), and H_2O_2 were magnetically stirred for 6 h. A sample aliquot was centrifuged at 10,000 rpm and absorbance spectra of the supernatant were measured in the 400–700 nm region using a UV–Vis spectrophotometer.

3.3. Antinociceptive Efficacy

The antinociceptive efficacy of REEW-GNs in Swiss albino mice was determined using Eddy's hot plate method. Experimental animals were divided into five groups (*n* = 6): Group I received 10 mL/kg.bw of normal saline, Group II received 10 mg/kg.bw of diclofenac sodium while Group III, IV, and V received 50, 100, and 200 mg/kg.bw of REEW-GNs, respectively. Mice with extreme baseline latencies (5 s > X > 30 s) were eliminated from the study. To avoid paw damage, cut-off period of 15 s was observed [46]. Response time in the form of flicking of fore or hind limbs and jumping was recorded at 55 ± 2 °C after 0, 30, 60, and 90 min of drug administration. The experimental animals were dealt with as per standard procedures of international guidelines for animal studies during the entire period of study [47].

3.4. Gastrointestinal Propulsion Bioassay

In vivo gastrointestinal propulsion bioassay was carried out on Swiss albino mice. The fore night fasted animals were divided into five groups of (*n* = 6): Group I received 10 mL/kg. b.w of normal saline, p.o; Group II received 10 mg/kg. b.w of atropine sulfate, p.o; Group III, IV, and V received 50, 100, and 200 mg/kg.bw of REEW-GNs, respectively (p.o). Animals were fed with 0.2 mL of activated charcoal after 15 min of drug administration. After 30 min of charcoal treatment, animals were sacrificed by cervical dislocation, dissected, and the intestine was cut down from pyloric to caecum [48,49]. The distance traveled by the charcoal relative to the total intestinal length was measured as percent propulsion using the following equation:

$$PP = \frac{DT}{DL} \times 100 \tag{2}$$

where PP stands for percent intestinal propulsion, DT stands for distance traversed by the charcoal, and TL is the total intestinal length.

Inhibition (%) of propulsion was calculated relative to negative control using the relation:

$$\text{Propulsion inhibition } (\%) = 100 \left[1 - \left(\frac{A}{B} \right) \right] \tag{3}$$

where A is for PP of drug-treated group and B is for PP of saline-treated group.

The experimental animals were dealt with as per standard procedures of international guidelines for animal studies during the entire period of study [50].

3.5. Blood Serum Assay (ALT, AST, ALT, T.P, and Bilirubin Level)

Experimental animals (Swiss albino mice of either sex) were divided into six groups (*n* = 6 each): Group I received 10 mL/kg.bw of normal saline for seven days; Group II received 1 g/kg.bw of acetaminophen/paracetamol (PCM) for seven days; Group III received 25 mg/kg b.w Silymarin and 1 g/kg.bw of PCM for seven days and Groups IV, V, and VI received 100, 250 and 500 mg/kg.bw of REEW-GNs and 1 g/kg.bw of PCM, respectively, for seven days (p.o) [47]. On day 8, all experimental animals were anesthetized by mild ether. Blood samples were collected separately in sterile centrifuge tubes by cardiac puncture and allowed to coagulate, centrifuged at 1000 rpm for 10 min for serum separation. The collected serum was subjected to biochemical estimation of ALP, AST, ALT, total bilirubin, and total protein using enzymatic kits.

3.6. Antidiabetic Activity

Antidiabetic activity of REEW-GNs was evaluated in alloxan-induced diabetic rabbits. To induce diabetes, 150 mg/kg b.w of alloxan was injected (i.v) in all experimental animals and after seven days blood glucose level (BGL) was tested using a glucometer. Animals with BGL > 200 mg/dL were selected for experimentation. Hyperglycemic rabbits were divided into five groups (*n* = 6): Group I received 10 mL/kg b.w saline; Group II received

0.5 mg/kg b.w of metformin; Groups III, IV, and V received 100, 200, and 300 mg/kg b.w. of REEW-GNs, respectively. BGL was monitored at 0.5, 2, 4, 8, 12, and 24 h of drug administration using glucometer while collecting blood from marginal ear vein. In vivo studies were performed in accordance with the approved protocols in the Guide for the Care and Use of Laboratory Animals of the National Institutes of Health. All measures were taken to minimize animals suffering during blood collection and surgery by subjecting animals to ether anesthesia [51].

4. Conclusions

The green approach to nanoparticle synthesis offers numerous advantages, including eco-friendliness, ease of synthesis, and wide economic viability. The reducing potential of the phytochemicals present in *E. wallichii* rhizome for gold ions serves as the basis for the synthesis of phytogenic gold nanoparticles. Spherical GNs were synthesized through the reduction of Au^{3+} ions in a green and low-cost method, employing the REEW extract as stabilizing and reducing agent. The resulting REEW-capped GNs exhibited significant potential in restoring the normal state of intoxicated malfunctioning liver and pancreas, increasing the pain threshold, and inhibiting GI propulsion, making it a promising alternative to classical analgesics and antispasmodics. Moreover, the phytogenic GNs have tremendous potential for scavenging varieties of ROSs and might be helpful in combating oxidative degenerative disorders. Green synthesis of nanoparticles is a simple, cost-effective, environmentally benign, and pollutant-free approach to the treatment of various ailments. Furthermore, this technology can be extended to produce other important metal NPs and potentially replace conventional drug delivery systems. However, investigating and ensuring its biosafety in living systems should be taken into consideration; therefore, there is a dire need for further studies to ensure its safe applicability and sustainable preparation.

Author Contributions: Conceptualization, R.U. and S.B.; methodology, A.K., S.B. and M.N.K.; software, A.K., S.B. and R.U.; validation, A.K., R.U. and S.B.; formal analysis, A.K., S.B. and M.N.K.; investigation and resources, M.N.K.; data curation, M.N.K. and Q.N.; writing—original draft preparation, A.K., M.N.K.; writing—review and editing, S.B., M.N.K., A.M.A.M. and Q.N.; visualization, Q.N., A.M.A.M. and S.B.; supervision and project administration, R.U. All authors have read and agreed to the published version of the manuscript.

Conflicts of Interest: We all authors declare that there are no conflict of interest.

References

1. Fakruddin, M.; Hossain, Z.; Afroz, H. Prospects and applications of nanobiotechnology: A medical perspective. *J. Nanobiotechnol.* **2012**, *10*, 31. [CrossRef] [PubMed]
2. Ul Haq, T.; Ullah, R.; Khan, M.N.; Nazish, M.; Almutairi, S.M.; Rasheed, R.A. Seed Priming with Glutamic-Acid-Functionalized Iron Nanoparticles Modulating Response of Vigna radiata (L.) R. Wilczek (Mung Bean) to Induce Osmotic Stress. *Micromachines.* **2023**, *14*, 736. [CrossRef]
3. Kaviya, S.; Santhanalakshmi, J.; Viswanathan, B. Green Synthesis of Silver Nanoparticles Using *Polyalthia longifolia* Leaf Extract along with D-Sorbitol: Study of Antibacterial Activity. *J. Nanotechnol.* **2011**, *2011*, 152970. [CrossRef]
4. Bronstein, L.M.; Chernyshov, D.M.; Volkov, I.O.; Ezernitskaya, M.G.; Valetsky, P.M.; Matveeva, V.G.; Sulman, E.M. Structure and properties of bimetallic colloids form in polystyrene-block-poly-4-venylpyridine micelles: Catalytic behavior in selective hydrogenation of dehydrolinabol. *J. Catal.* **2000**, *196*, 302–314. [CrossRef]
5. Narayanan, K.B.; Sakthivel, N. Biosynthesis of gold nanoparticles by using *coriander* leaf extract. *Mater. Lett.* **2008**, *62*, 4588–4590. [CrossRef]
6. Shankar, S.S.; Rai, A.; Ahmad, A.; Sastry, M.J. Rapid synthesis of Au, Ag and bimetallic Au shell nanoparticles using Neem. *J. Colloid Interface Sci.* **2004**, *275*, 496–502. [CrossRef]

7. Song, J.Y.; Jang, H.K.; Kim, B.S. Biological synthesis of gold nanoparticles using *Magnolia kobus* and *Diopyros kaki* leaf extracts. *Process Biochem.* **2009**, *44*, 1133–1138. [CrossRef]

8. Alkilany, A.M.; Shatanawi, A.; Kurtz, T.; Caldwell, R.B.; Caldwell, R.W. Toxicity and cellular uptake of gold nanorads in vascular endothelium and smooth muscles of isolated rat blood vessel: Importance of surface modification. *Small* **2012**, *8*, 1270–1278. [CrossRef]

9. Hosny, M.; Fawzy, M.; El-Badry, Y.A.; Hussein, E.E.; Eltaweil, A.S. Plant-assisted synthesis of gold nanoparticles for photocatalytic, anticancer, and antioxidant applications. *J. Saudi Chem. Soc.* **2022**, *26*, 101419. [CrossRef]

10. Faryal, S.; Ullah, R.; Khan, M.N.; Ali, B.; Hafeez, A.; Jaremko, M.; Qureshi, K.A. Thiourea-capped nanoapatites amplify osmotic stress tolerance in Zea mays L. by conserving photosynthetic pigments, osmolytes biosynthesis and antioxidant biosystems. *Molecules* **2022**, *27*, 5744. [CrossRef]

11. Jakhmola, A.; Krishnan, S.; Onesto, V.; Gentile, F.; Profeta, M.; Manikas, A.; Battista, E.; Vecchione, R.; Netti, P.A. Sustainable synthesis and theoretical studies of polyhedral gold nanoparticles displaying high SERS activity, NIR absorption, and cellular uptake. *Mater. Today Chem.* **2022**, *26*, 101016. [CrossRef]

12. Saha, K.; Agasti, K.; Li Rotello, V.M. Gold nanoparticles in chemical and biological sensing. *Chem. Rev.* **2011**, *112*, 2739–2779. [CrossRef] [PubMed]

13. Sen, A.; Batra, A. Evaluation of antimicrobial activity of different solvent extracts of medicinal plant: *Melia azedarach* L. *Int. J. Curr. Pharm. Res.* **2012**, *4*, 67–73.

14. Rao, C.N.R.; Cheetham, A.K. Science and technology of nanomaterials: Current status and future prospects. *J. Mater. Chem.* **2011**, *11*, 2887–2894. [CrossRef]

15. Jakhmola, A.; Vecchione, R.; Onesto, V.; Gentile, F.; Profeta, M.; Battista, E.; Manikas, A.C.; Netti, P.A. A theoretical and experimental study on l-tyrosine and citrate mediated sustainable production of near infrared absorbing twisted gold nanorods. *Mater. Sci. Eng. C* **2021**, *118*, 111515. [CrossRef]

16. Huang, X.; El-Sayed, M.A. Gold nanoparticles: Optical properties and implementations in cancer diagnosis and photothermal therapy. *J. Adv. Res.* **2010**, *1*, 13–28. [CrossRef]

17. Kalimuthu, K.; Venkataraman, D.; Babu, R.K.P.; Muniasamy, K.; Selvaraj, B.M.K.; Bose, K.; Sangiliyandi, G. Biosynthesis of Gold and Silver nanoparticles using *Bravibacteriumcasei*. *Colloids Surf. B Biointerfaces* **2010**, *77*, 257–262.

18. Geddes, C.D.; Parfenov, A.; Gryczynski, I.; Lakowicz, J.R. Luminescent blinking of gold nanoparticles. *Chem. Phys. Lett.* **2003**, *380*, 269–272. [CrossRef]

19. Gupta, N.; Vishnoi, G.; Wal, A.; Wal, P. Medicinal value of *Euphorbia tirucalli*. *Sys. Rev. Pharm.* **2013**, *4*, 40–46. [CrossRef]

20. Ali, I.; Naz, R.; Khan, W.N.; Gul, R.; Choudhary, M.I. Biological screening of different root extracts of *Euphorbia wallichii*. *Pak. J. Bot.* **2009**, *41*, 1737–1741.

21. Ul-Haq, I.; Ullah, N.; Bibi, G.; Kanwal, S.; Ahmad, M.S.; Mirza, B. Antioxidant and cytotoxic activities and phytochemical analysis of *Euphorbia wallichii* root extract and its fractions. *Iran. J. Pharm. Res. IJPR* **2012**, *11*, 241. [PubMed]

22. Hassan, A.; Yaqoob, U.; Nawchoo, I.A.; Gulzar, S.; Mohi-Ud-Din, G.; Nazir, S.; Ashraf, A. Conspectus of phytochemical constituents of *Euphorbia wallichii* Hook. f.: A review. *Res. Rev. J. Bot.* **2016**, *5*, 24–31.

23. Phull, A.R.; Ali, A.; Ali, A.; Abbasi, S.; Zia, M.; Khaskheli, M.H.; Kamal, M.A. Synthesis of Silver Nanoparticles using *Euphorbia wallichii* Extract and Assessment of their Bio-functionalities. *Med. Chem.* **2020**, *16*, 495–506. [CrossRef]

24. Ullah, R.; Ud Din, S.; Muhammad, Z.; Shah, S.; Jan, S.A. Biological efficacy of phyto-synthetic silver nanoparticles using ethanol extract of *Euphorbia wallichii* Hook Rhizome as bio-reductant and surfactant. *Trop. J. Pharm. Res.* **2018**, *17*, 1903–1909. [CrossRef]

25. Kelesidis, G.A.; Gao, D.; Fabian, H.L.; Pratsinis, S.E. Light Excitation by Agglomerates of Gold nanoparticles: A plasmon ruler for sub-10 nm interparticle distance. *Anal. Chem.* **2022**, *94*, 5310–5316. [CrossRef]

26. Karthick, V.; Kumar, V.G.; Dhas, T.S.; Singaravelu, G.; Sadiq, A.M.; Govindaraju, K. Effect of biologically synthesized gold nanoparticles on alloxan-induced diabetic rats-an in vivo approach. *Colloids Surf. B Biointerfaces* **2014**, *122*, 505–511. [CrossRef]

27. Zhang, Q.; Dan, H.; Xueying, W.; Mengyu, X.; Ziling, L.; Lihong, W.; Janak, L. Pathak. Gold nanomaterials for oral cancer diagnosis and therapy: Advances, challenges, and prospects. *Mater. Today Bio.* **2022**, *15*, 100333. [CrossRef]

28. National Research Council. *Guide for the Care and Use of Laboratory Animals, 8th ed*; The National Academies Press: Washington, DC, USA, 2011; pp. 1–246.

29. Okokon, J.E.; Bawo, M.B.; Mbagwu, H.O. Hepatoprotective activity of *Mammea africana* ethanol stem bark extract. *Avicenna J. Phytomed.* **2016**, *6*, 248–259.

30. Gupta, A.K.; Chitme, H.; Dass, S.K.; Misra, N. Hepatoprotective activity of *Rauwolfia serpentine* rhizome in paracetamol intoxicated rats. *J. Pharmacol. Toxicol.* **2006**, *1*, 82–88. [CrossRef]

31. Marotta, F.; Yadav, H.; Gumaste, U.; Helmy, A.; Jain, S.; Minelli, E. Protective effect of a phytocompound on oxidative stress and DNA fragmentation against paracetamol-induced liver damage. *Ann. Hepatol.* **2009**, *8*, 50–56. [CrossRef]

32. Nithianantham, K.; Shyamala, M.; Chen, Y.; Latha, Y.; Jothy, S.L.; Sasidharan, S. Hepatoprotective potential of *Clitoria ternatea* leaf extract against paracetamol induced damage in mice. *Molecules* **2011**, *16*, 10134–10145. [CrossRef]

33. Dash, D.K.; Yeligar, V.C.; Nayak, S.S.; Ghosh, T.; Rajalingam, D.; Sengupta, P. Evaluation of hepatoprotective and antioxidant activity of *Ichnocarpus frutescens* (Linn.) R.Br. on paracetamol-induced hepatotoxicity in rats. *J. Pharmaceut. Res.* **2007**, *6*, 755–765.

34. Cedeño-Pinos, C.; Jiménez-Monreal, A.M.; Quílez, M.; Bañón, S. Polyphenol Extracts from Sage (*Salvia lavandulifolia* Vahl) By-Products as Natural Antioxidants for Pasteurised Chilled Yoghurt Sauce. *Antioxidants* **2023**, *12*, 364. [CrossRef]

35. Santa-Cecília, F.V.; Vilela, F.C.; da Rocha, C.Q.; Dias, D.F.; Cavalcante, G.P.; Freitas, L.A.S.; Giusti-Paiva, A. Anti-inflammatory and antinociceptive effects of *Garcinia brasiliensis*. *J. Ethnopharmacol.* **2011**, *133*, 467. [CrossRef]
36. Das, S.C.; Bhadra, S.; Roy, S.; Saha, S.K.; Islam, M.S.; Bachar, S.C. Analgesic and Anti-inflammatory Activities of Ethanolic Root Extract of *Swertia chirata* (Gentianaceae). *Jordan J. Biol. Sci.* **2012**, *5*, 31–36.
37. Wang, S.Y.; Lan, X.; Xiao, J.; Yang, J.; Kao, Y.; Chang, S. Anti Inflammatory Activity of *Lindera erythrocarpa* Fruits. *Phytother. Res.* **2008**, *22*, 213–216. [CrossRef]
38. Fürst, S.; Zádori, Z.S.; Zádor, F.; Király, K.; Balogh, M.; László, S.B.; Hutka, B.; Mohammadzadeh, A.; Calabrese, C.; Galambos, A.R.; et al. On the Role of Peripheral Sensory and Gut Mu Opioid Receptors: Peripheral Analgesia and Tolerance. *Molecules* **2020**, *25*, 2473. [CrossRef]
39. Kidd, B.; Urban, L. Mechanisms of inflammatory pain. *B. J. Anaesth.* **2001**, *87*, 3–11.
40. Somasundaram, S.; Sigthorsson, G.; Simpson, R.J.; Watts, J.; Jacob, M.; Tavares, I.A.; Rafi, S.; Roseth, A.; Foster, R.; Price, A.B.; et al. Uncoupling of intestinal mitochondrial oxidative phosphorylation and inhibition of cyclooxygenase are required for the development of NSAID—Enteropathy in the rat. *Aliment. Pharmacol. Ther.* **2000**, *14*, 639. [CrossRef]
41. Shaheen, T.I.; El-Naggar, M.E.; Hussein, J.S.; El-Bana, M.; Emara, E.; El-Khayat, Z. Antidiabetic assessment; in vivo study of gold and core-shell silver-gold nanoparticles on streptozotocin-induced diabetic rats. *Biomed. Pharmacother.* **2016**, *83*, 865–875.
42. Lin, L.; Guan, H.; Li, R.; Liao, X.; Zhao, F.; Wang, M.; Li, J.; Xu, G.; He, X.; Zhang, J.; et al. Auriculatone Sulfate Effectively Protects Mice Against Acetaminophen-Induced Liver Injury. *Molecules* **2019**, *24*, 3642. [CrossRef] [PubMed]
43. Halliwell, B.; Clement, M.V.; Long, L.H. Hydrogen peroxide in the human body. *FEBS Lett.* **2000**, *486*, 10–13. [CrossRef] [PubMed]
44. Halliwell, B.; Gutteridge, J.M.C. The antioxidants of human extracellular fluids. *Arch. Biochem. Biophys.* **1990**, *280*, 18. [CrossRef] [PubMed]
45. Apak, R.; Özyürek, M.; Güclu, K.; Çapanoglu, E. Antioxidant Activity/Capacity Measurement. Reactive Oxygen and Nitrogen Species (ROS/RNS) Scavenging Assays, Oxidative Stress Biomarkers, and Chromatographic/Chemometric Assays. *J. Agric. Food Chem.* **2016**, *64*, 1046–1070. [CrossRef]
46. Saritha, K.; Saraswathi, U. Antioxidant activity of gold nanoparticles synthesized using Lemna minor. *World J. Pharm. Sci.* **2014**, *2*, 1545–1551.
47. Shamkuwar, P.B.; Pawar, D.P. Antidiarrhoeal and Antispasmodic Effect of *Berberis Aristata*. *Int. J. Pharm. Phytochem. Res.* **2013**, *5*, 24–26.
48. Nagajothi, P.C.; Lee, K.D. Synthesis of plant mediated silver nanoparticles using *Dioscorea batatas* rhizome extract and evaluation of their antimicrobial activities. *J. Nanomater.* **2011**, *2011*, 49. [CrossRef]
49. Sallie, R.; Tredger, J.M.; Williams, R. Drugs and the liver. Part 1: Testing liver function. Biopharm. *Drug Dispos.* **1991**, *12*, 251–259. [CrossRef]
50. Ezike, A.C.; Akah, P.A.; Okoli, C.O.; Ufere, I.K.; Ezeudu, E.; Okoye, C.F.; Ashara, C.; Igbokwe, I.N. Studies on Gastrointestinal Effects Of Desmodium Velutinum: A Traditional Remedy For Diarrhea. Am. J. Pharmacol. *Toxicol.* **2014**, *9*, 114–124.
51. Franzotti, E.M.; Santos, C.V.F.; Rodrigues, H.M.L.S.; Mourao, R.H.V.; Andrade, M.R.; Antoniolli, A.R. Anti-inflammatory, analgesic activity and acute toxicity of Sida cordifolia L. (Malva-branca). *J. Ethnopharmacol.* **2000**, *72*, 273–278. [CrossRef]